Microstructural evolution in a 5024 aluminum alloy processed by ECAP with and without back pressure

A. Mogucheva [a,*], E. Babich [a], B. Ovsyannikov [b], R. Kaibyshev [a]

[a] Belgorod State University, 85 Pobedy, Belgorod 308015, Russia
[b] Kamensk-Uralsky Metallurgical Works J.S.Co, Kamensk-Uralsky, Zavodskaya, 5, 623405, Russia

Keywords:
Equal channel angular processing
Aluminum alloys
Grain refinement
EBSD
Microhardness measurement

A B S T R A C T

The microstructural evolution of an Al–4.57Mg–0.2Sc–0.09Zr–0.64Mn (in wt%) alloy processed by equal channel angular pressing (ECAP) without and with back pressure (BP) was investigated at 300 °C. ECAP up to a strain of $\varepsilon \sim 12$ without and with BP provided the formation of fine recrystallized grains with a size of ~870 nm; their volume fraction was 77% and 86%, respectively. The application of a BP ensures the homogeneity of the billet processed and leads to an increased rate of continuous dynamic recrystallization (CDRX). The positive effect of BP on grain refinement through ECAP is attributed to the fact that BP facilitates the formation of deformation bands during the first to second passes. These deformation bands evolve uniformly on the macroscale of whole billets and mesoscale of initial grains and then rapidly transform into chains of recrystallized grains under further straining. The uniformity of deformation banding ensures an extensive decrease in the unrecrystallized fraction with strain. The mechanisms of new grain evolution, as well as factors promoting grain refinement, are discussed.

1. Introduction

Equal-channel angular pressing is a highly suitable technique for the fabrication of none age-hardenable alloys belonging to the Al–Mg–Sc system with ultrafine-grained (UFG) structure [1–4] that provides enhanced mechanical properties [5,6]. A fully recrystallized structure with an average grain size of ~1 μm may be easily produced in these alloys through ECAP at a temperature of 300 °C [3,5,7]. For soft materials, ECAP is a relatively simple procedure that can be used to achieve exceptional grain refinement by repetitive pressing up to very high strain [1,8]; therefore, this processing technique is highly attractive for the enhancement of such materials' mechanical properties. In ECAP, the nature of the imposed deformation is simple shear [1]; plastic deformation is localized in the small area around the intersection of the two channels [1,9,10]. The uniformity of the strain distribution in the shear plane ensures the homogeneity of the deformation structure and, therefore, the mechanical properties of the material [1,9,10]. However, a non-uniform shear deformation usually takes place under ECAP [1]. As a result, the deformation microstructure is essentially inhomogeneous on the macroscale of a billet [11]. The presence of a dead-metal zone in the outer corner of an ECAP die leads to the spread of the deformation away from the shear zone, which disturbs the material flow dramatically [1,8,10]. Currently, it is well-accepted that simple shear deformation is extremely important for the formation of a UFG structure [1,12–15]; the deviation from simple shear makes the grain refinement process slow. As a result, the formation of a fully recrystallized structure requires severe deformation [1–4]. ECAP has a great potential for being scaled up to produce relatively large samples, and the non-uniformity of shear deformation is an important obstacle to the implementation of this technique for commercial use [1,12].

Recently, incorporating a back pressure into the ECAP operation has been successfully adopted for diminishing the non-uniformity of simple shear and eliminating billet defects [1,8–11,13–18]. BP lowers the total strain, which is necessary to produce a uniform UFG structure due to the increase in the width of the deformation zone and change in the mode of deformation to simple shear [1,8–10,13,14,18]. The deformation zone becomes more like a localized shear band, which is typical of a rigid, perfectly-plastic body [1]. The application of a BP during ECAP leads to a reasonable homogeneity of the deformation structure on the cross-sectional plane, with the exception of a small and continuous region lying adjacent to the bottom edge of the billet [1,8,15]. These factors facilitate extensive grain refinement in Sc-modified aluminum alloys [5,16]. In addition, the application of a BP leads to the filling of the outer corner, and a consequent removal of the dead zone [1] and well-known defect of a leading end of a workpiece [1,10]. The latter is highly suitable for the commercial-scale-up of the ECAP technique [1,10,16,18].

However, to date, limited information is available regarding the effect of a BP on the rate of grain refinement under ECAP [1,16] and the uniformity of the deformation structure [11,17].

* Corresponding author. Tel./fax: +74 72 258 5456.
E-mail address: mogucheva@bsu.edu.ru (A. Mogucheva).

Recently, it was shown that the effect of BP on the homogeneity of plastic deformation depends on material parameters [14,15,18], and therefore, it is necessary to carry out a systematic examination of the role of a BP during grain refinement in commercial aluminum alloys. The aim of the present study was to consider microstructural evolution in an Al–Mg–Sc–Zr alloy subjected to ECAP with and without a BP. This alloy is an advanced material for cryogenic applications in high-value components, primarily for use in the aerospace industry. An important current objective is therefore to process this material for achieving uniform mechanical properties in the cross-section of billets. The levels of homogeneity, which may be achieved in billets processed by ECAP, are very important for the commercial application of the ECAP technique [1,11,16–18]. Therefore, in this report, specific attention will be paid to the examination of the effect of BP on uniformity of billets processed by ECAP.

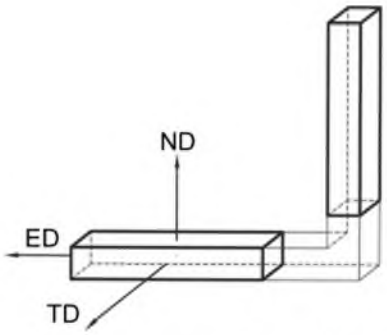

Fig. 1. Schematic illustration of the processed billet; ED, ND and TD denote extrusion direction, normal direction and transverse direction, respectively.

2. Material and experimental procedure

The material used in this investigation was a wrought AA5024 (4.57Mg–0.2Sc–0.09Zr–0.64Mn in wt%) supplied by Kamensk-Uralsky Metallurgical Works J.S.Co (Kamensk-Uralsky, Russia). The AA5024 was produced by continuous casting. Ingots with initial dimensions of ∅620 mm were subjected to homogenization annealing at 370 ± 10 °C for 12 h. Next, the ingot was extruded at a temperature of 380 °C into a billet with a rectangular cross section and dimensions of 155 × 255 mm^2. Rectangular samples with dimensions of 20 × 20 × 100 mm^3 and 14 × 14 × 80 mm^3 were machined from the central part of the extruded billet parallel to the extrusion direction (ED) (Fig. 1). ECAP with a BP of about 100 MPa and without BP was conducted at 300 °C using isothermal dies with square internal cross-section of 20 × 20 mm^2 and 14 × 14 mm^2, respectively. Each die had a channel intersection angle of 90°. Deformation through these dies produces a strain of ~1 on each passage. The rods were pressed up to strains of ~1, ~2, ~4, ~8 and ~12. The samples were rotated by 90° around the Z axis between each pass along the same direction, i.e., the route B_c [1] was used. The pressing speed was approximately 2 mm/s. The total time, during which each billet with the aforementioned dimensions was held at the deformation temperature between ECAP passes was ~2 min per each extrusion pass.

The Vickers microhardness (HV) was measured using a regular rectilinear grid pattern with a spacing of 1 mm between each separate position to evaluate the homogeneity of the deformation microstructure. The individual values of HV were plotted in the form of contour maps displaying the variation in the local microhardness over the sectional surface of each billet processed by ECAP in accordance with methods described in [11,17] in detail.

The details of sample preparation for microstructural observations have been reported in previous works [2,3]. Metallographic

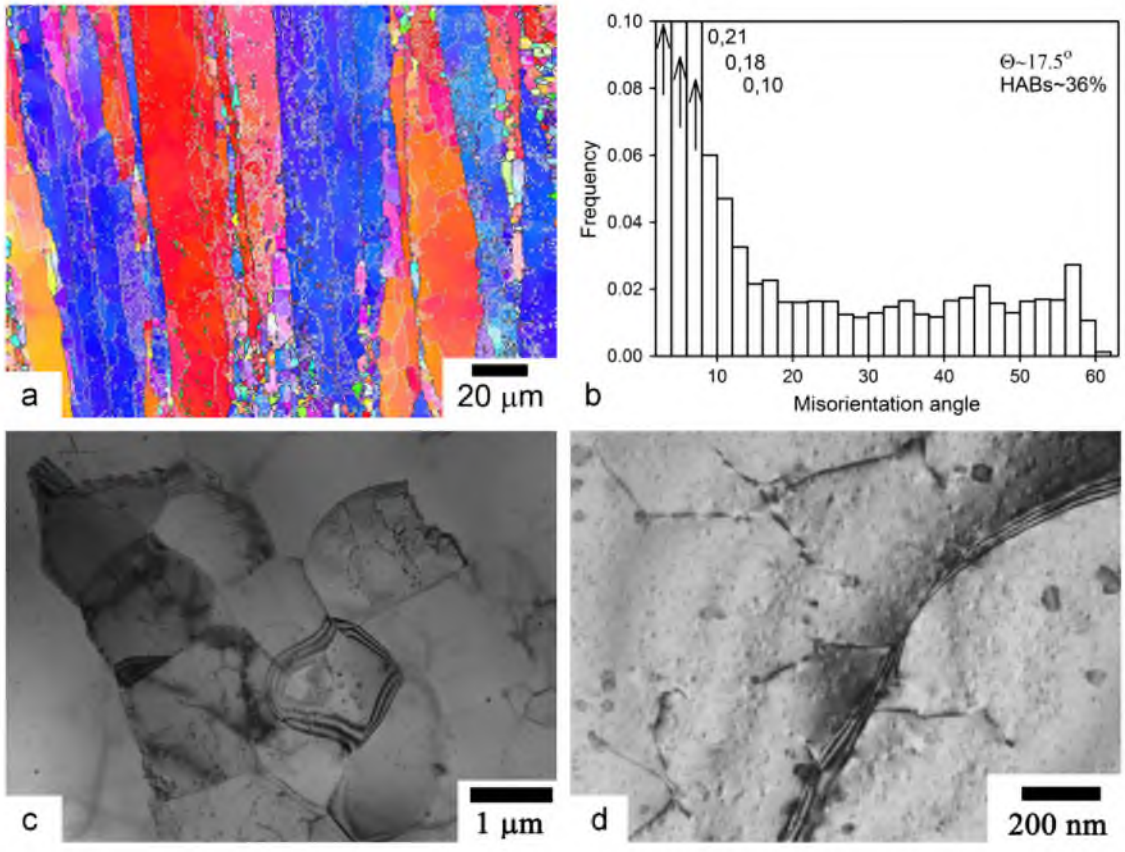

Fig. 2. Initial microstructure of the 5024 alloy after hot extrusion.

observations were carried out using an Olympus GX70 microscope. Thin foils were examined using a JEM-2100 transmission electron microscope (TEM) with a double-tilt stage and an accelerating potential of 200 kV. The dislocation density was estimated by counting individual dislocations crossing the thin foil surface [19]. The misorientations on the (sub)grain boundaries were studied using the conventional Kikuchi-line technique via TEM [20]. Orientation imaging microscopy (OIM) with automated indexing of electron back scattering diffraction (EBSD) patterns was performed in a FEI Quanta 600FEG scanning electron microscope (SEM) with OIM analysis software provided by TexSem Lab Inc. Notably, black and white lines on the EBSD maps indicate high-angle boundaries (HABs) ($\geq 15^\circ$) and low-angle boundaries (LABs) (2°–15°), respectively. The average grain size was measured by the OIM software, and the average (sub)grains size was measured by the mean linear intercept method. The terms 'grain' and '(sub)grains' are used to define the crystallites, which are entirely delimited by the HABs and partly by LABs and partly by HABs, respectively [19]. The volume fraction of grains was deemed to be the 'recrystallized' fraction.

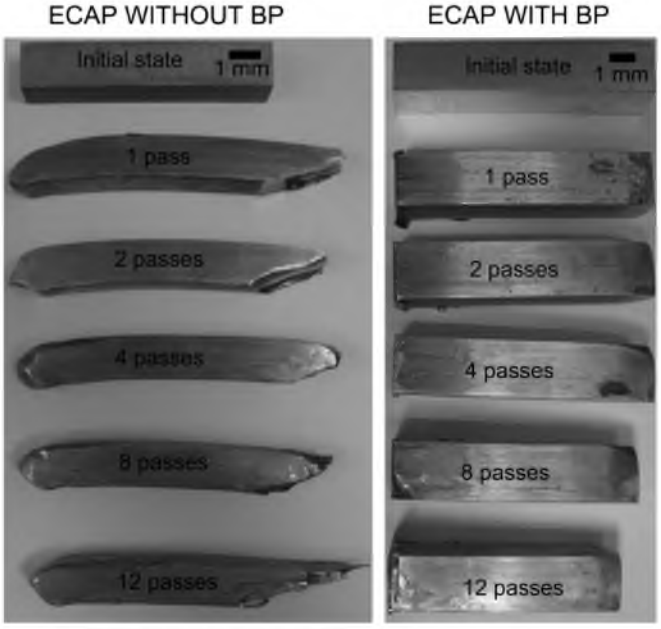

Fig. 3. Billets processed by ECAP with and without BP up to different strains.

3. Experimental results

3.1. Microstructure before ECAP

The typical hot extruded microstructure of the 5024 alloy was observed in the alloy's initial state. The coarse grains are highly elongated toward ED (Fig. 2a) and have dimensions of ~200 and ~20 μm along the longitudinal and transverse directions, respectively. The chains of fine grains having an equiaxed shape and an

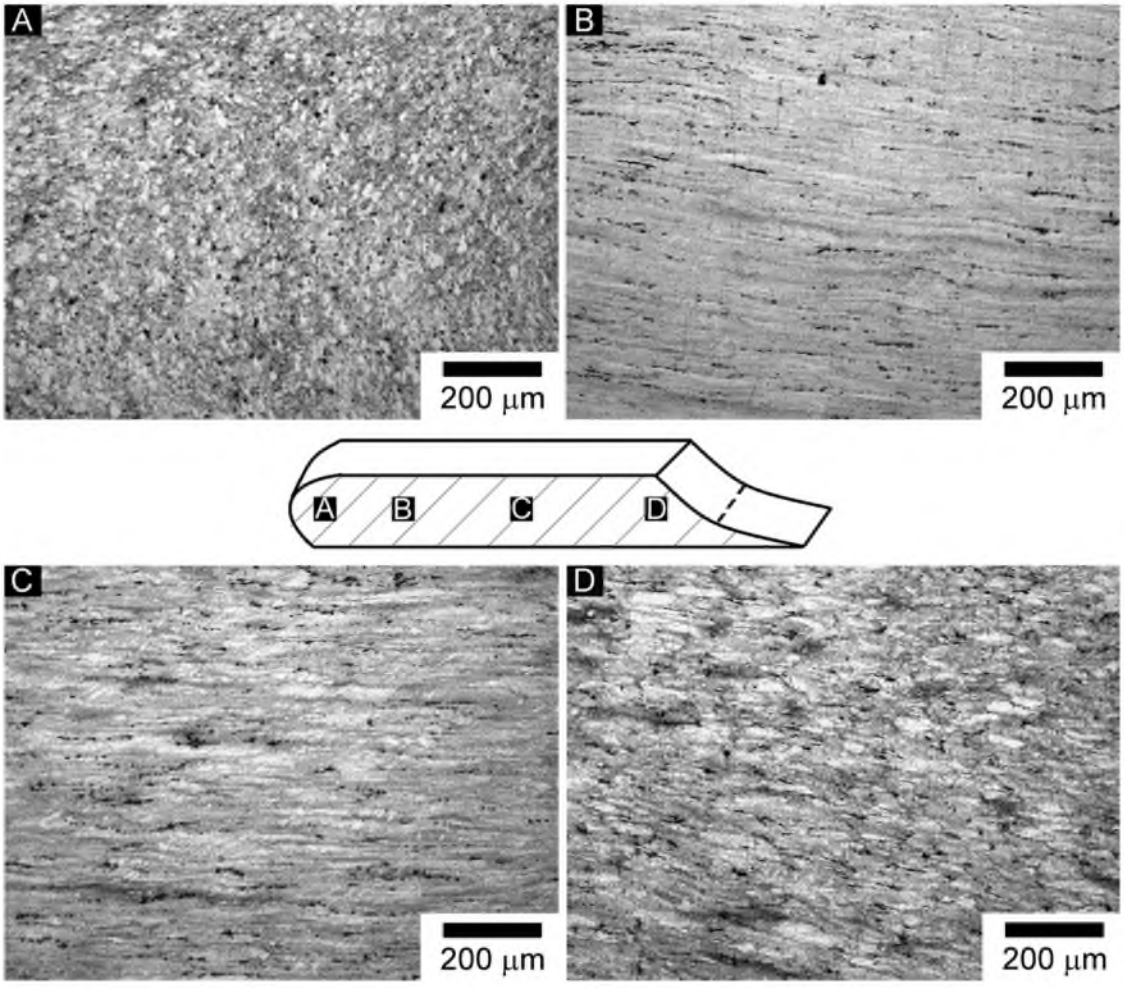

Fig. 4. Typical deformation microstructure after 12 passes of ECAP without BP. A–D denote the areas of metallographic observations.

average size of ~2 μm are located along separate initial HABs (Fig. 2a). The fraction of HABs is ~36%, and the average misorientation is ~17.5° (Fig. 2b). Extended boundaries having low-to-moderate misorientation were observed within the interiors of original grains. Most of these boundaries are planar. These LABs comprise deformation bands (DBs), which are aligned along the extrusion direction as the original boundaries. In addition, deformation bands delimited by the planar LABs and original HABs could be found in the vicinity of initial boundaries (Fig. 2a). The lattice dislocation density ($\rho \sim 10^{13}\ m^{-2}$) is not particularly high (Fig. 2c). Subgrains exhibiting an essentially equiaxed shape with an average size of ~1.2 μm were rarely observed (Fig. 2c). Coherent dispersoids of the $Al_3(Sc,Zr)$-phase with an average size of ~20 nm and equiaxed shape are uniformly distributed within grain interiors (Fig. 2d).

3.2. Effect of BP on the homogeneity of the microstructure and microhardness distribution

3.2.1. Microstructural homogeneity

Fig. 3 shows the billet before and after ECAP without and with the BP for 1, 2, 4, 8 and 12 cycles. It is readily observed that ECAP without BP leads to a significant waste of the material; at $\varepsilon \sim 12$, significant workpiece defects including trailing ends and visible leading ends could be observed. It is apparent that the fraction of wasted material increases with increasing strain. This processing technique is not suitable for commercial use due to the relatively small material yield. It was observed that the application of the BP eliminated billet defects; ECAP with a BP produces nearly defect-less workpieces and is highly suitable for commercialization.

Figs. 4 and 5 show a schematic diagram of the areas, where the deformed microstructures were examined. A well-defined difference between the microstructure evolved within the billet body and within the leading end and the trailing end was found in billets subjected to ECAP without BP. However, the deformation microstructure throughout the billet body is reasonably homogeneous. In contrast, metallographic observations show that the deformation microstructure evolved in different areas of the billet subjected to ECAP with BP is essentially the same. Areas of the billet subjected to 12 passes are clearly distinguished by the direction along which unrecrystallized grains are elongated. However, no remarkable difference in the fraction of recrystallized grains between different areas in the billet was found (Fig. 5).

3.2.2. Microhardness distribution

Color-coded contour maps representing microhardness distribution are shown in Figs. 6–8. The reference directions, i.e. ED, TD and ND, and cross-sections of A–D were selected as shown in Figs. 1 and 4, 5, respectively. Figs. 6 and 7 depict the transverse sections of the billets processed up to $\varepsilon \sim 12$ by ECAP without and with BP, respectively. For ECAP without BP the four cross-sections

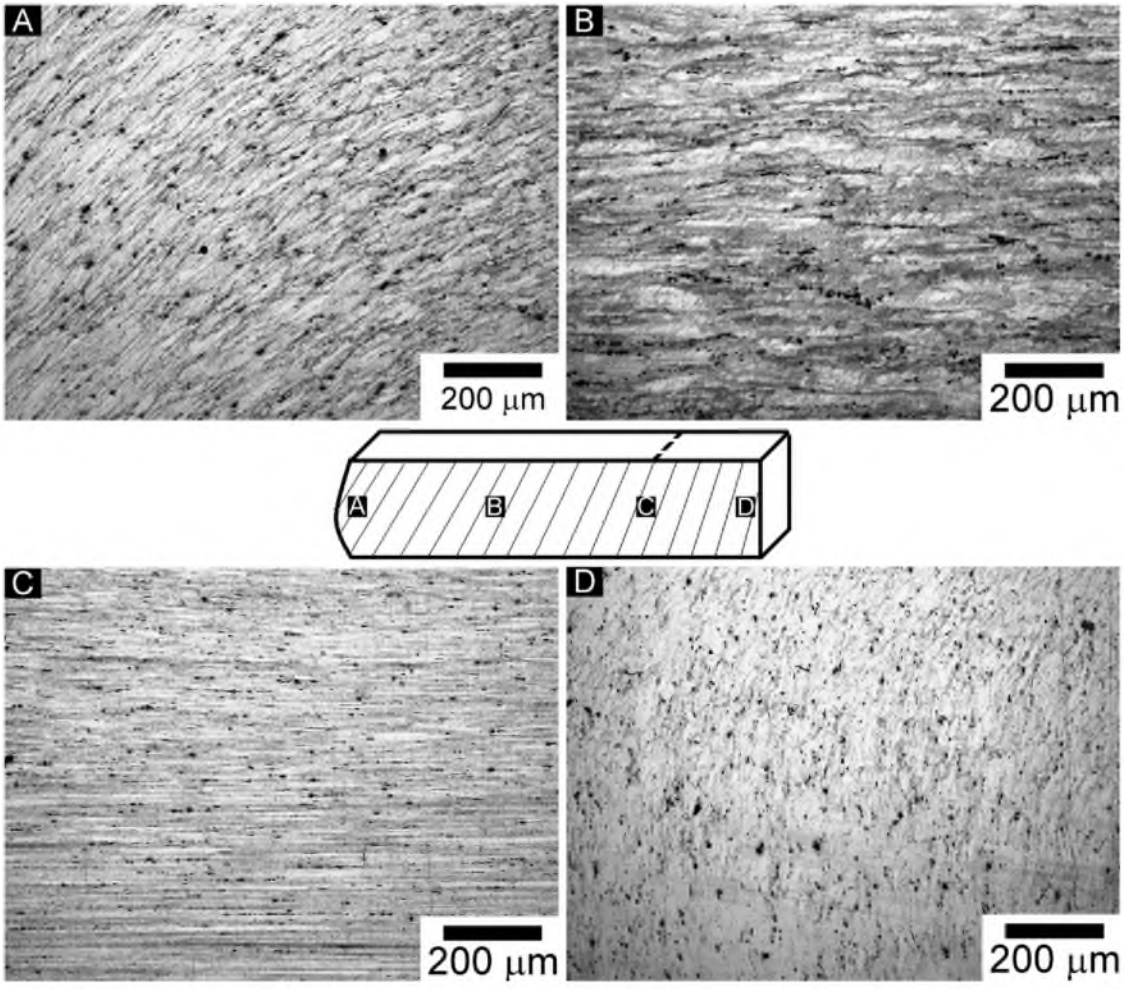

Fig. 5. Typical deformation microstructures after 12 passes of ECAP with BP. A–D denote the areas of metallographic observations.

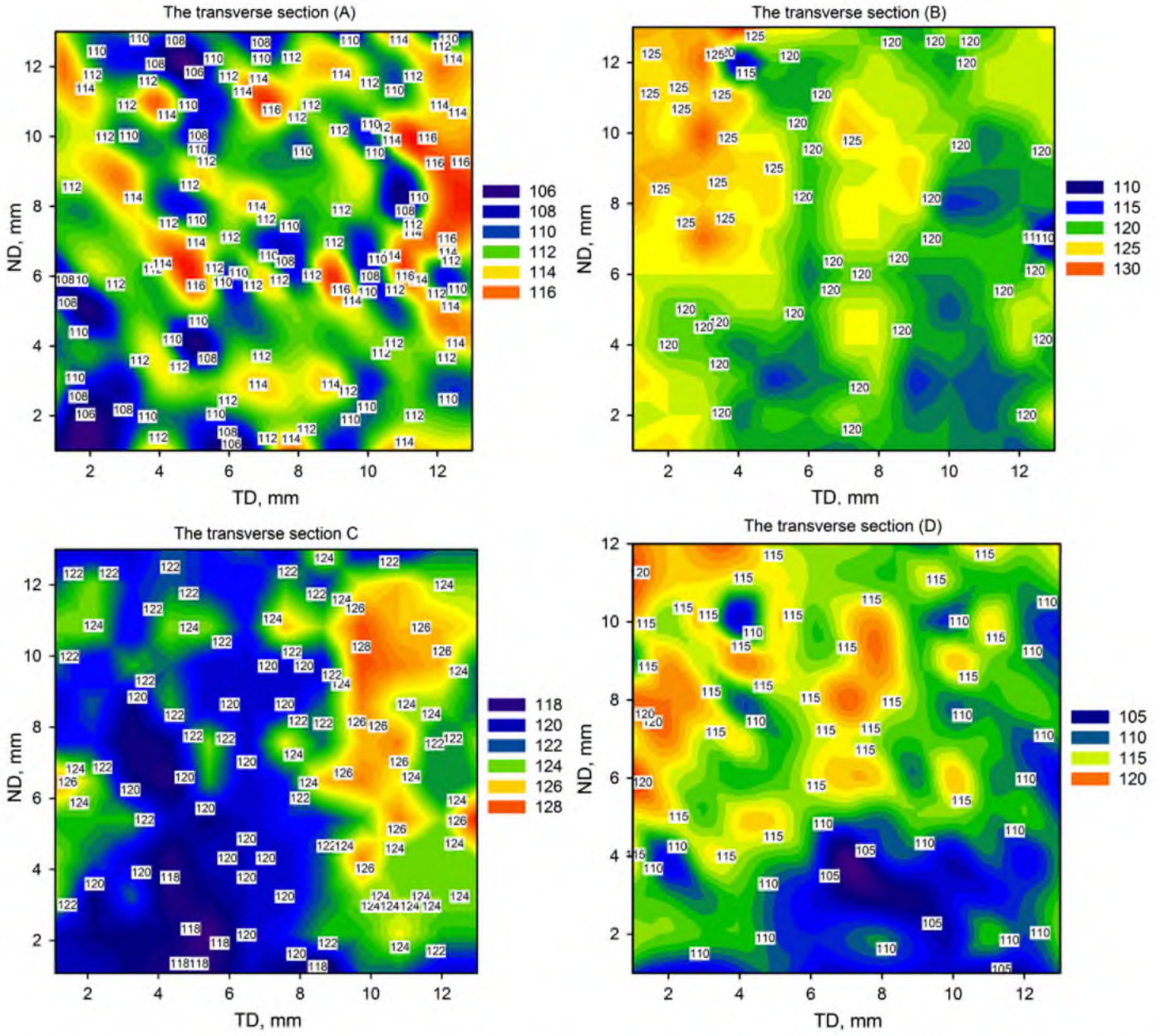

Fig. 6. Color-coded contour maps showing the Vickers microhardness through the transverse cross-sections of A–D denoted in Fig. 5 of the 5024 alloy subjected to ECAP without BP up to $\varepsilon \sim 12$.

are presented to show the difference in microhardness along the extrusion direction of the pressed billet. For ECAP with BP, only one cross-section is presented; the microhardness distribution through the other cross-section planes is almost the same and is essentially independent of the location on the section within the billet body. Fig. 8 shows the longitudinal section of the 5024 alloy after 12 passes of ECAP with and without the BP.

The microhardness over the entire cross-sections of the AA5024 subjected to ECAP without BP is non-uniform throughout the whole billet and varies from ~110 to 130 HV; the average value is ~125 HV. Lower hardness values were found near the front and rare defects were observed (sections A and D in Fig. 4). For instance, near the leading end defect, the hardness changes from 105 to 120 HV; the average value is 112 HV. The billet is inhomogeneous along the longitudinal section (Fig. 8a), with higher values of microhardness occurring near the top surface of the billet and lower values occurring in the vicinity of the lower surface. Minor variations in hardness take place within the central core regions of the as-pressed billet.

In contrast, the microhardness distribution of the transverse cross-section (section B in Fig. 5) of the billet subjected to ECAP with BP is reasonably homogeneous (Fig. 7). Minor variations in microhardness from 130 to 138 HV are observed between different areas over the entire cross-section. The average microhardness value is 135 HV. Thus, incorporating the BP slightly increases the average microhardness and provides a significant benefit in reducing the scattering of microhardness values over transverse cross-sections. It is worth emphasizing that the deviations in the microhardness over the billet subjected to ECAP with BP are a factor of 2 lower than those over the billet processed by ECAP without BP. The formation of reasonably homogeneous deformation structure within the whole billet subjected to ECAP with

BP results in the uniform distribution of microhardness over the longitudinal section (Fig. 8a and b). Thus, the application of the BP highly improves the homogeneity of the pressed billets.

3.3. Deformation microstructure

3.3.1. ECAP without back pressure

Typical EBSD maps, misorientation distribution and TEM micrographs of the deformation microstructure are shown in Figs. 9–11, respectively. At $\varepsilon\sim1$, the elongation of original grains along the shear direction and the formation of extended LABs (Fig. 9a) in a manner similar to that under preceding extrusion (Fig. 1a) was observed. In addition, extensive serration of initial boundaries occurs (Fig. 9a). Deformation bands delimited by LABs with a spacing of 5.3 μm are observed on the misorientation map within separate initial grains (Fig. 9a). Chains of fine grains with an average size of ~1.2 μm evolve on the initial boundaries (Figs. 9a and 11a) that provide a relatively high portion of HABs (30.3%) (Fig. 10a).

At $\varepsilon\sim2$, the chains of fine grains having an essentially equiaxed shape and an average size of ~0.9 μm are rarely observed along some initial boundaries; deformation bands delimited by LABs evolve within the grain interiors (Fig. 9b). The volume fraction of true grains is relatively low (~4%). EBSD data show that the HAB portion (30.5%) and average misorientation (15.5°) do not change due to the formation of numerous LABs with $\theta\geq2^\circ$ within the interiors of initial grains (Figs. 10b and 11b). These LABs comprise the aforementioned deformation bands elongated along the last shear direction, and the spacing between dislocation boundaries decreases to 4.1 μm. TEM observation revealed a high dislocation density ($\rho\sim3.4\times10^{14}\,m^{-2}$) and the formation of crystallites having an equiaxed shape and an average size of ~410 nm (Fig. 11b'). These grains exhibit well-defined extinction contours (Fig. 11b'). It is worth noting that the lattice dislocation density within initial grains and that within deformation-induced grains or (sub)grains are essentially the same. All deformation-induced boundaries in the vicinity of an initial boundary exhibit low-angle origin (Fig. 11b).

Deformation to $\varepsilon\sim4$ leads to the formation of a partially recrystallized structure consisting of chains of grains with an average size of ~870 nm located along initial boundaries and where the former deformation bands occurred (Fig. 9c). Crystallites delimited by HABs and LABs with an average size of ~1 μm or less exhibit an essentially equiaxed shape. The volume fraction of submicrometer scale true grains is ~18%; the HAB population and average misorientation reach ~62% and ~26.4°, respectively (Fig. 10c). TEM observation revealed a reduced dislocation density ($\rho\sim1\times10^{14}\,m^{-2}$); moreover, the deformation bands tend to transform into chains of crystallites measuring 450 nm in size, which acquire an essentially equiaxed shape (Fig. 11c). It is worth noting that the size of the crystallites determined by TEM is a factor of ~2 smaller than that obtained by the EBSD technique. With further deformation to $\varepsilon\sim8$, the volume fraction of fine

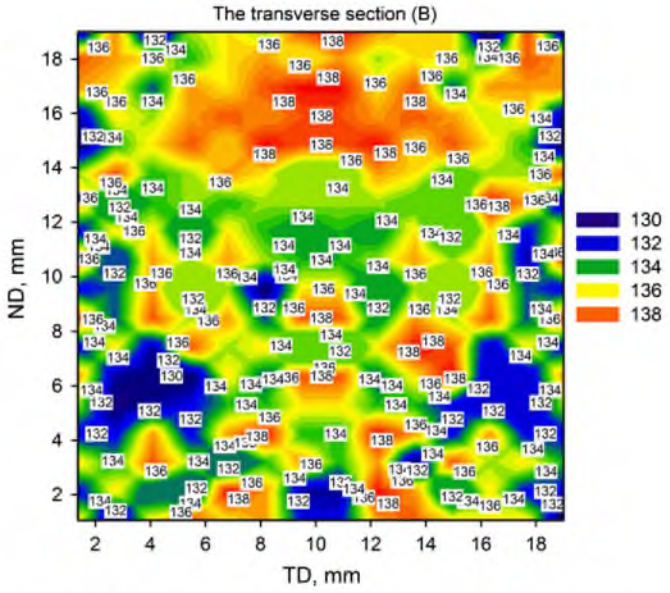

Fig. 7. Color-coded contour maps showing the Vickers microhardness through the B transverse cross-section (Fig.5) of the 5024 alloy subjected to ECAP with BP up to $\varepsilon\sim12$.

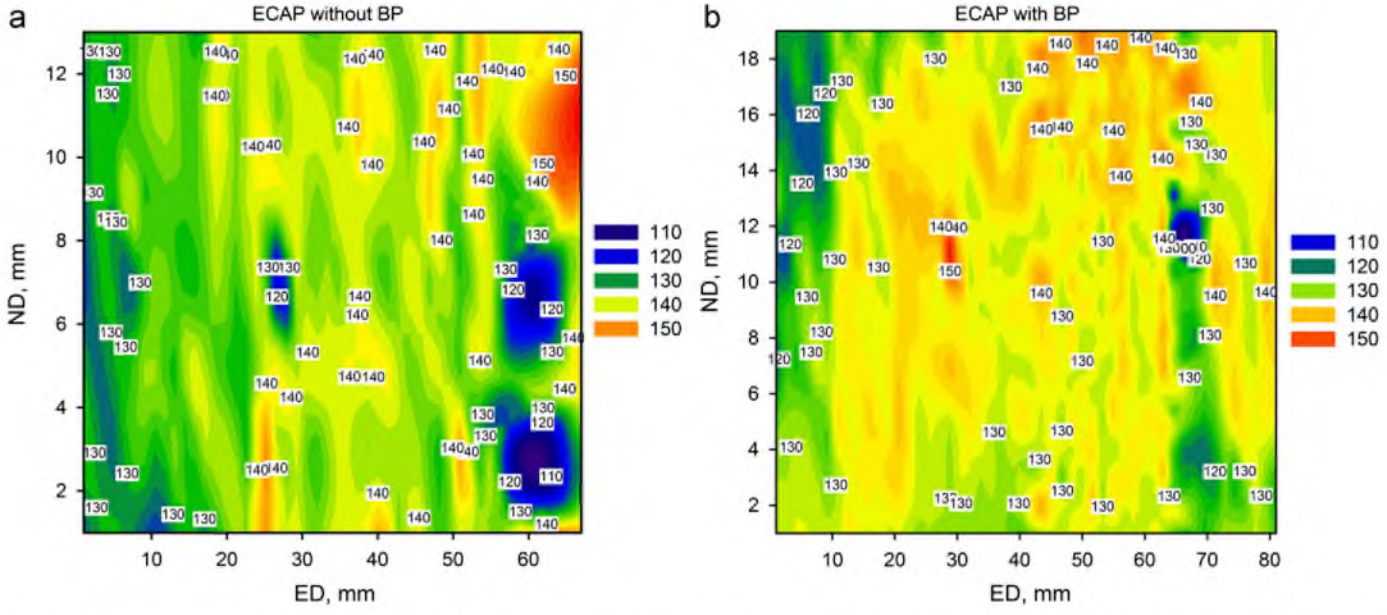

Fig. 8. Color-coded contour maps showing the Vickers microhardness through the longitudinal sections of the 5024 alloy subjected to ECAP (a) without B P and (b) with BP up to $\varepsilon\sim12$.

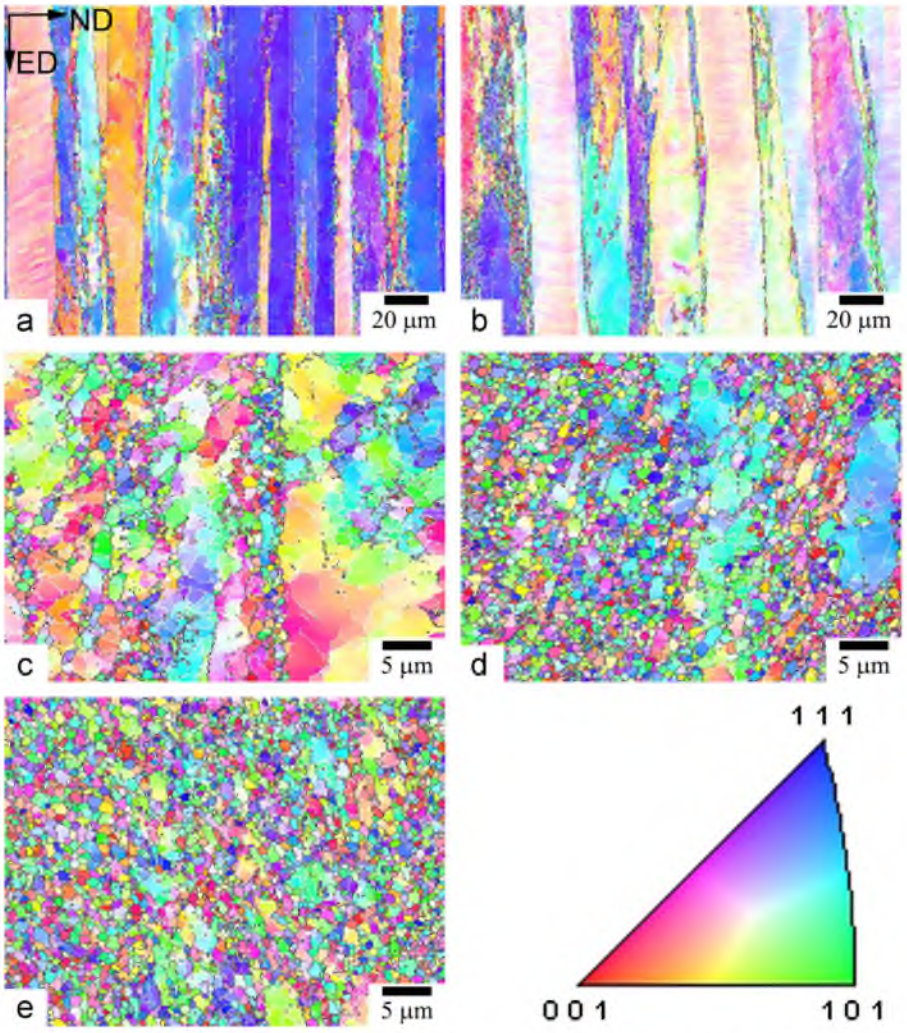

Fig. 9. EBSD misorientation maps obtained from samples subjected to ECAP without BP up to: (a) $\varepsilon\sim1$; (b) $\varepsilon\sim2$; (c) $\varepsilon\sim4$; (d) $\varepsilon\sim8$; and (e) $\varepsilon\sim12$.

grains and average misorientation increase to ~67% and ~28.5°, respectively (Figs. 9d and 10d). The dislocation density again increases up to $\rho\sim1.8\times10^{14}\ m^{-2}$ (Fig. 11d). The volume fraction of new grains increases, and the average size of these grains remains unchanged. Almost all smaller than 1 μm acquired an equiaxed shape (Fig.11d).

At $\varepsilon\sim12$, no formation of a fully recrystallized structure is attained (Fig. 9e); areas of recrystallized grains with an average size of ~870 nm alternate with unrecrystallized areas with sizes ranging from 2 to 4 μm. Notably, most of the recrystallized grains are composed of chains (Fig. 9e). An increase in total strain from ~8 to ~12 yields no remarkable changes in the HAB portion or average misorientation (Fig. 10e) despite a significant decrease in the volume fraction of unrecrystallized areas (Fig. 9e). This may be attributed to the extensive formation of LABs within the remainder of the initial grains (Fig. 11e'). The volume fraction of recrystallized grains increases to 77 pct. It is worth noting that most of the crystallites are grains having an equiaxed shape and containing a high density of lattice dislocations ($\rho\sim2\times10^{14}\ m^{-2}$) (Fig. 11e).

3.3.2. *ECAP with back pressure*

Data regarding structural characterization are presented in Figs. 12–14. The main difference between microstructural evolution under ECAP without and with the BP consists in the rate of the formation of deformation bands within the interiors of initial grains. In the early stages of processing with BP, the deformation bands are the main characteristic feature of the deformation structure. At $\varepsilon\sim1$, most of the initial grains are subdivided by deformation bands on structural elements with an average thickness of ~3.9 μm and delimited by LABs (Fig. 12a). As a result of the extensive formation of deformation bands, an average misorientation of 12.6° and HAB portion of ~23% (Fig. 13a) are less than those values measured in the 5024 alloy subjected to ECAP without BP (Fig. 10a). TEM observation showed that the formation of chains of the crystallites measuring 500 nm and 600 nm along the longitudinal and transverse directions, respectively, takes place within the interiors of initial grains after the first pass (Fig. 14a). Their portion is almost similar to that in the 5024 alloy subjected to ECAP without BP up to $\varepsilon\sim4$. Thus, the BP greatly accelerates the formation of submicron-scale crystallites. At $\varepsilon\sim1$, no effect of the BP on the overall dislocation density was observed ($\rho\sim5\times10^{13}\ m^{-2}$).

Further deformation to $\varepsilon\sim2$ leads to an increase in the number of deformation bands (Fig. 12b); the average misorientation and HAB portion increase to ~15.7° and 32% (Fig. 13b), respectively. The formation of deformation bands delimited by LABs was observed within the interiors of the initial grains; the thicknesses of these bands range from 100 to 800 nm (Fig. 14b and b'). It can

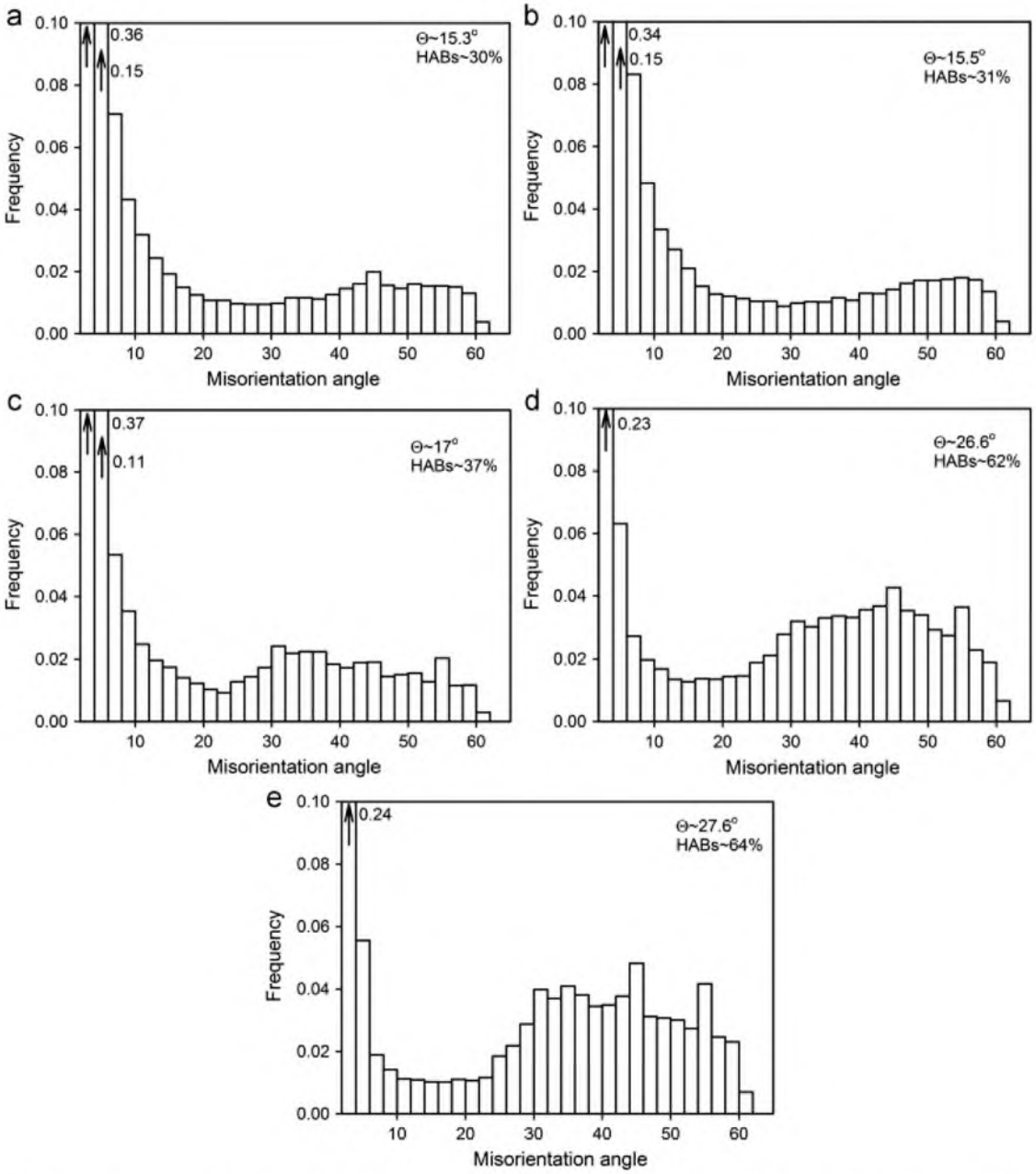

Fig. 10. Misorientation distribution obtained from samples subjected to ECAP without BP up to: (a) $\varepsilon\sim1$; (b) $\varepsilon\sim2$; (c) $\varepsilon\sim4$; (d) $\varepsilon\sim8$; and (e) $\varepsilon\sim12$.

be observed that the number of transverse boundaries within thin deformation bands is significantly higher than that within thick bands; the formation of numerous narrow deformation bands highly facilitates their subdivision into rectangular crystallites by the further formation of transverse boundaries. The average dislocation density decreases to $\rho\sim2\times10^{14}\,m^{-2}$. Thus, at $\varepsilon\leq2$, a number of deformation bands and the dislocation density increase with strain concurrently (Fig. 14b and b'). At $\varepsilon\sim2$, the average dislocation density after ECAP with BP is lower, and the density of deformation bands is higher compared with that generated after ECAP without back pressure. Therefore, the BP highly promotes the formation of deformation bands; the increase in the HAB portion originates from the grain subdivision process by deformation banding.

At $\varepsilon\sim4$, the HAB portion and average misorientation increase to ~62% and ~26°, respectively (Figs. 12c and 13c). However, this deformation structure is a partially recrystallized structure. Unrecrystallized areas subdivided by LABs on relatively coarse subgrains can be found (Figs. 12c and 14c); their volume fraction is ~46%. It seems that compared to the situation created by ECAP without BP, with BP the remains of the initial grains are subjected to extensive recrystallization. The transformation of deformation bands delimited by LABs into chains of (sub)grains exhibiting an essentially equiaxed shape was almost completed at this strain (Fig. 14c).

At $\varepsilon\sim8$, an almost fully recrystallized structure evolves (Figs. 12d and 13d); the HAB portion and average misorientation reach ~67.5% and 28.5°, respectively. It can be observed that recrystallized grains are composed of well-defined chains (Fig. 12d). The volume fraction of recrystallized grains with an average size of 890 nm is as high as 74%. TEM revealed the formation of grains with an essentially equiaxed shape and average size of ~390 nm (Fig. 14d).

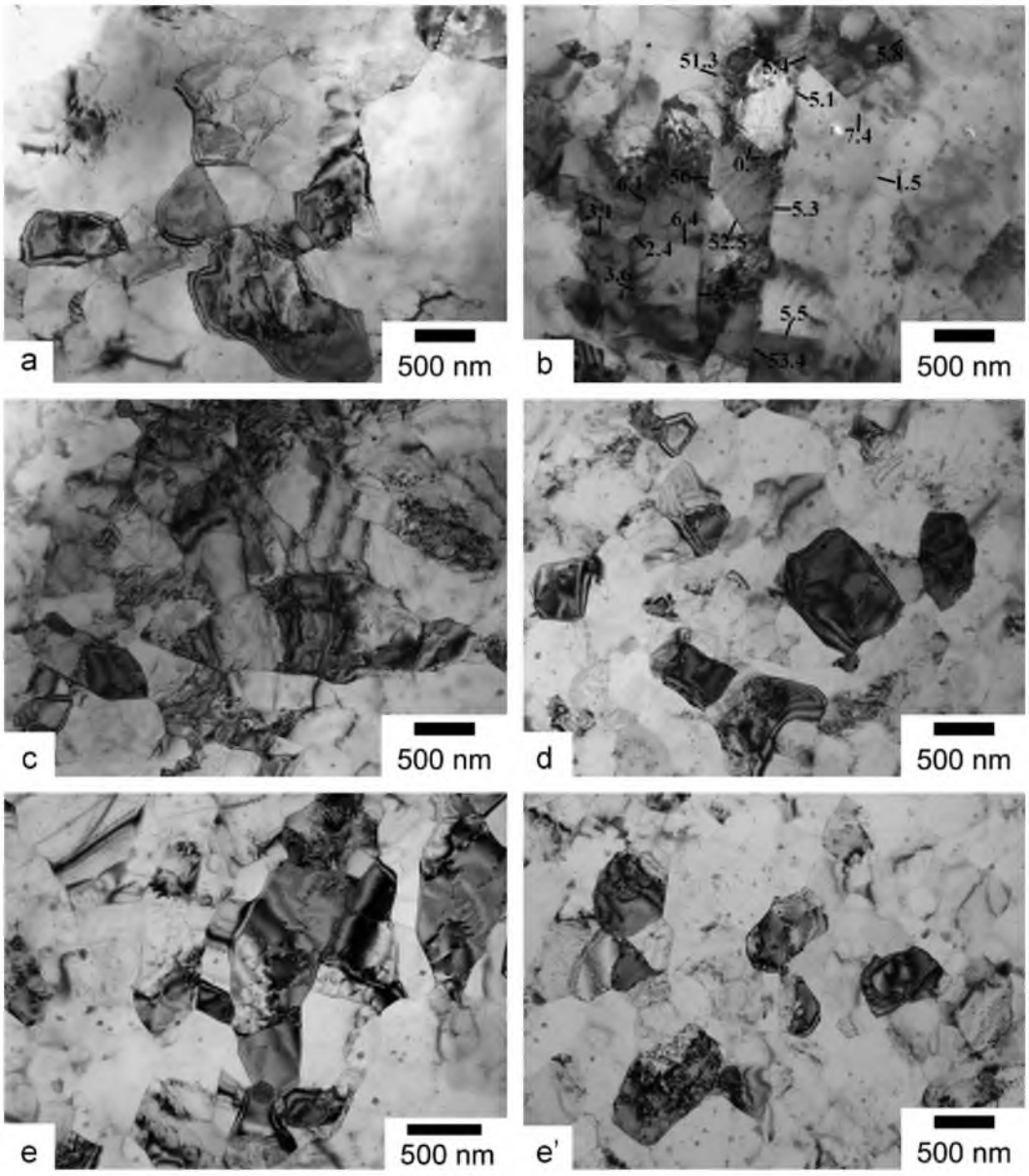

Fig. 11. TEM micrographs obtained from samples subjected to ECAP without BP up to: (a) $\varepsilon\sim1$; (b) $\varepsilon\sim2$; (c) $\varepsilon\sim4$; (d) $\varepsilon\sim8$; and (e and e') $\varepsilon\sim12$.

Further deformation to $\varepsilon\sim12$ provides significant refinement of unrecrystallized areas (Fig. 12e). Their largest dimension does not exceed 3 μm; these areas alternate with recrystallized grains (Fig. 12e). However, an increase in total strain from ~8 to ~12 yields only slight increases in the HAB portion and average misorientation (Fig. 13e). TEM observation shows that the average size of recrystallized grains does not change (Fig. 14e). It is apparent that a fully recrystallized structure evolves beyond $\varepsilon\sim12$. The lattice dislocation density within recrystallized grains remains almost unchanged ($\rho\sim1.4\times10^{14}$ at $\varepsilon\sim4$ and $\rho\sim1.2\times10^{14}\,m^{-2}$ at $\varepsilon\sim12$). No accumulation of lattice dislocation at the boundaries of recrystallized grains takes place (Fig. 14c–e); their boundaries exhibit well-defined extinction contours that are indicative of a very low density of lattice dislocations trapped by grain boundaries [21].

3.4. *Parameters of microstructure as a function of strain*

The effect of strain on the average size of strain-induced crystallites, average misorientation (Θ_{av}), portion of HABs (V_{HAB}), fraction of recrystallized grains (V_{rec}) and lattice dislocation density (ρ) are summarized in Fig. 15. There is no quantitative effect of BP on the strain dependencies of structural parameters, which show a similar trend under ECAP with and without BP. However, the incorporation of BP into the ECAP operation highly accelerates the process of grain refinement, especially within the strain interval 1–4 (Fig. 15). For instance, the average size of recrystallized grains after ECAP without BP gradually decreases along the transverse and longitudinal directions from 6 μm to 1.2 μm and from 10 μm to 1.1 μm, respectively, when pressing is continued from 1 to 8 passes (Fig. 15a), and under ECAP with BP, rapid changes in microstructure occur within the first 4 passes: the grain size along both directions decreases down to 0.88 μm at $\varepsilon\sim4$ (Fig. 15b). Upon further strain, no significant difference in the size of crystallites could be observed under ECAP with or without BP (Fig. 15a and b). The average size of strain-induced crystallites in the samples subjected to ECAP with BP is slightly lower (~450 nm) than that in the samples subjected to ECAP without BP (~500 nm) due to the difference in thickness of the deformation bands.

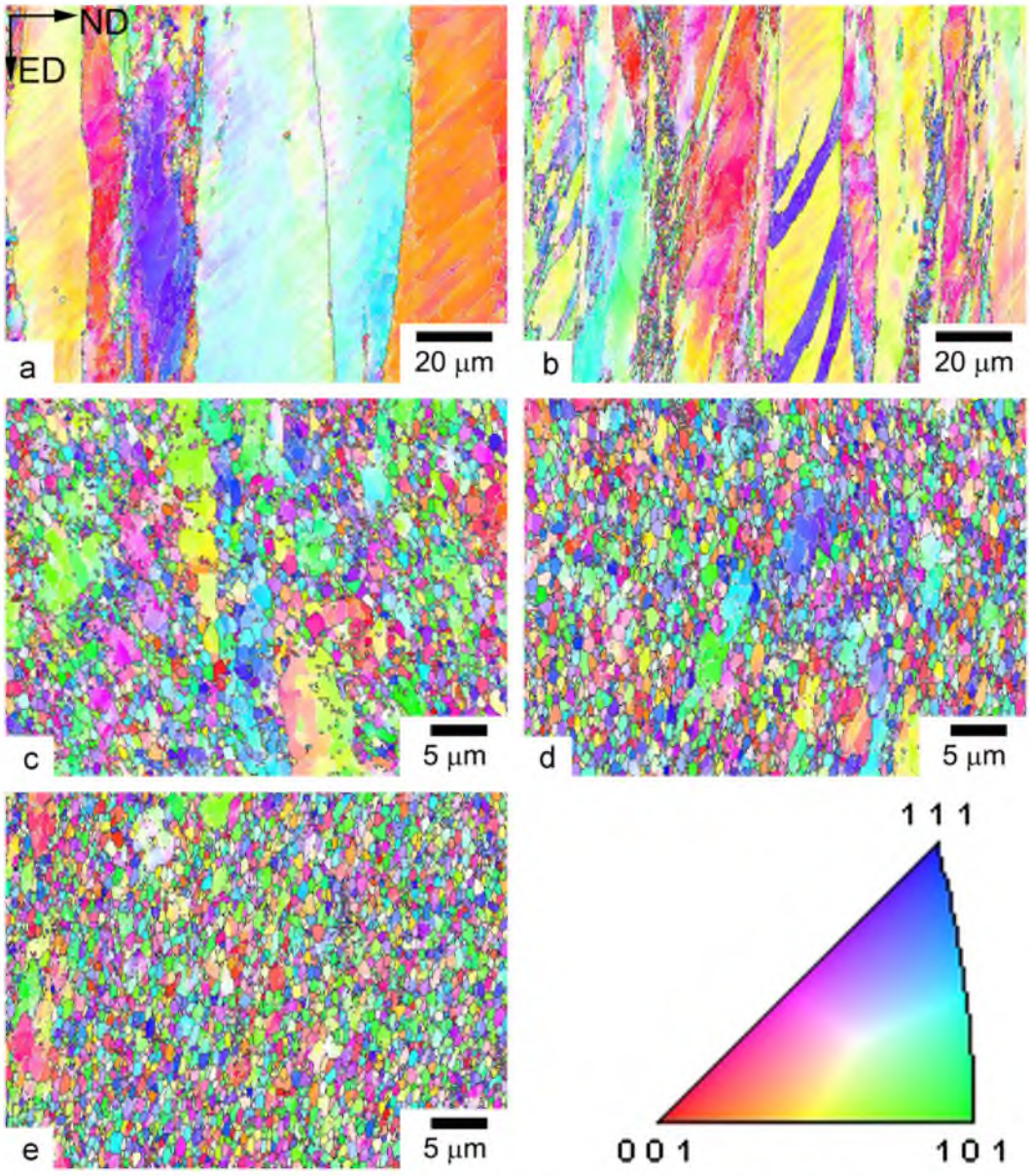

Fig. 12. EBSD misorientation maps obtained from samples subjected to ECAP with BP up to: (a) $\varepsilon\sim1$; (b) $\varepsilon\sim2$; (c) $\varepsilon\sim4$; (d) $\varepsilon\sim8$; and (e) $\varepsilon\sim12$.

The dependence of the average misorientation, Θ_{av}, (Fig. 15c), volume fraction of recrystallized grains, V_{rec}, (Fig. 15d) and HABs portion, F_{HAB}, (Fig. 15e) on strain reveals three distinct stages of microstructural changes that occur during ECAP [22–24]. First, a rapid increase in the Θ_{av} and F_{HAB} (Fig. 15c and e) of deformation-induced boundaries takes place beyond $\varepsilon\sim2$ with BP and only beyond $\varepsilon\sim4$ without BP. It is worth noting that in the present study we calculated the misorientation of all grain boundaries. As a result, this stage is characterized by a slow decrease in these values. The V_{rec} value increases to a plateau within the first 2 passes under ECAP with and without BP. Second, a rapid increase in Θ_{av}, V_{rec}, and F_{HAB} values (Fig. 15c–e) takes place during strains higher than a critical strain of ~2. However, the application of BP accelerates the recrystallization process at Stage II and shifts Stage III to lower strain. It is clearly observed that under ECAP with BP Stage II terminates at $\varepsilon\sim4$, while under ECAP without BP Stage II extends up to $\varepsilon\sim8$ (Fig. 15c–e). Moreover, the average misorientation and portion of HABs in the samples subjected to ECAP with BP up to $\varepsilon\sim4$ are higher than those in the samples subjected to ECAP without BP up to $\varepsilon\sim8$. Third, a gradual increase in Θ_{av} and F_{HAB} to higher saturation values ultimately takes place (Fig. 15c and e); the fraction of recrystallized grains tends to approach 100%. Thus, BP highly promotes the grain refinement process. These data correlate with the effect of strain on recrystallized grain size (Fig. 15a and b). The rate of recrystallization is similar under ECAP with and without BP. However, the deformation structure that evolved under ECAP with BP could transform into a fully recrystallized structure during the first 8 passes, in contrast the structure observed under ECAP without BP.

The effect of BP on the dislocation density vs strain dependence (Fig. 15f) is correlated with the effect of BP on the rate of recrystallization (Fig. 15c–e). A strong increase in the lattice dislocation density takes place within the first 2 passes. Further deformation up to 4 passes leads to a decrease in the ρ value to $\sim1.5\times10^{14}\,m^{-2}$. Upon further strain, the lattice dislocation

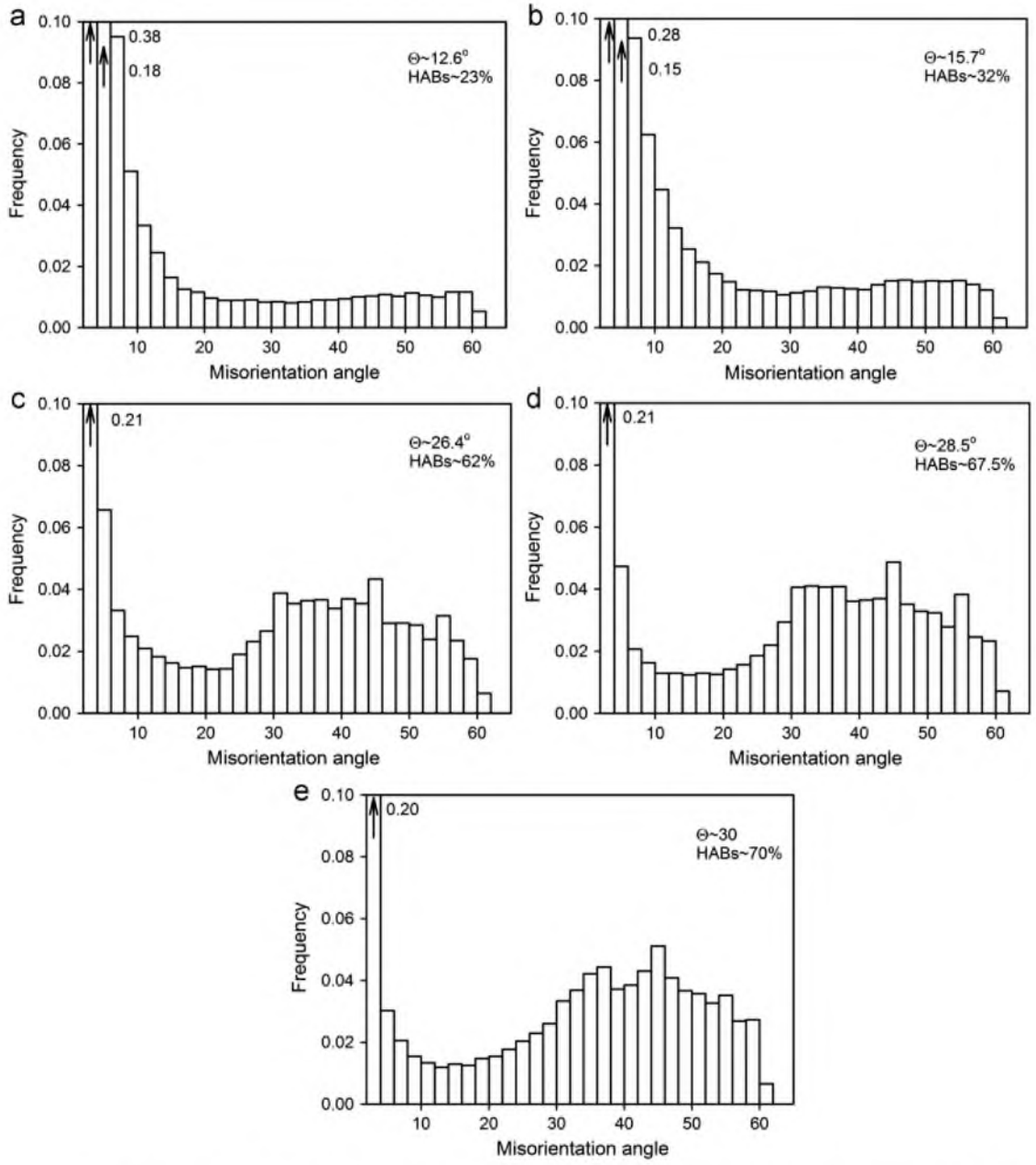

Fig. 13. Misorientation distribution obtained from samples subjected to ECAP with BP up to: (a) $\varepsilon \sim 1$; (b) $\varepsilon \sim 2$; (c) $\varepsilon \sim 4$; (d) $\varepsilon \sim 8$; and (e) $\varepsilon \sim 12$.

density undergoes an insignificant increase up to an apparent saturation value of $\sim 2 \times 10^{14}\,m^{-2}$ under ECAP without BP. In contrast, under ECAP with BP the lattice dislocation density remains essentially unchanged with strain. It is apparent that BP facilitates the accumulation of lattice dislocations within deformation-induced boundaries [19].

4. Discussion

The inspection of microstructural evolution shows that continuous dynamic recrystallization (CDRX) [19,22–25] contributes significantly to grain refinement under ECAP with and without BP. This conclusion is supported by the well-accepted fact [26,27] that if the portion of HABs in an aluminum alloy sample reaches ≥ 0.64, the sample is considered to have undergone CDRX, which involves the formation of stable 3D arrays of deformation LABs followed by their gradual transformation into HABs upon straining that leads to the continuous increase in misorientation across deformation-induced boundaries (Fig. 16) [19,25,26,28]. In aluminum alloys at intermediate temperatures the initial formation of 3D arrays of LABs is the slowest process which controls the overall rate of CDRX [19,22,23]. This process can occur in two ways [19,28,29]: (I) rearrangement of lattice dislocations forming pile-ups by climb or cross-slip leads to the formation of subgrains with an equiaxed shape (Fig. 17a); (II) the formation of deformation bands [28,29] delimited by geometrically necessary boundaries (GNBs) [30] with low-to-moderate misorientation and planar shape (Fig. 17b). Under further deformation the rearrangement of lattice dislocations within these GNBs may lead to their transformation into subgrain boundaries inducing no or low long-range elastic stress fields [31]. The application of the BP strongly facilitates the evolution of LABs through

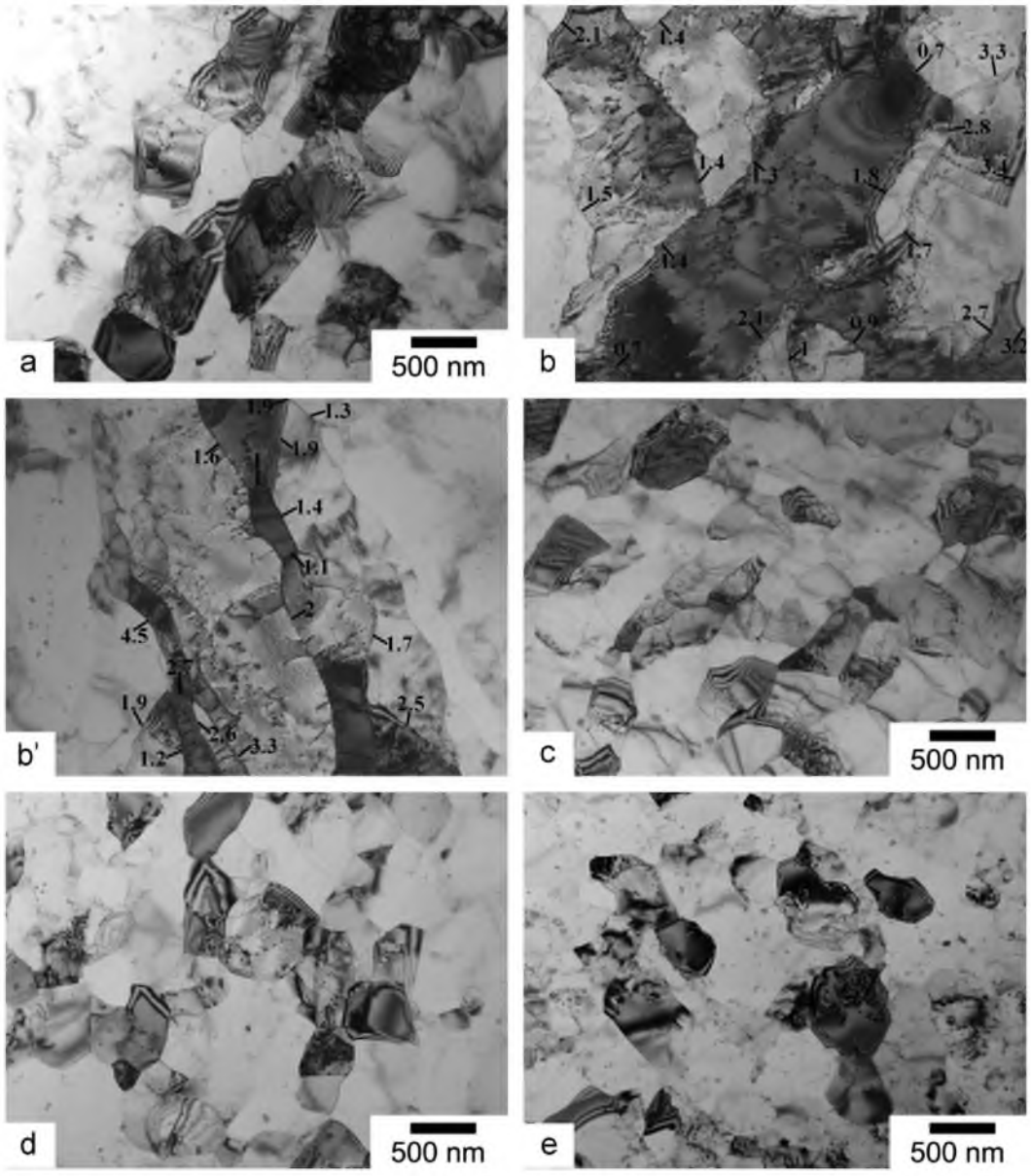

Fig. 14. TEM micrographs obtained from samples subjected to ECAP with BP up to: (a) $\varepsilon \sim 1$; (b and b') $\varepsilon \sim 2$; (c) $\varepsilon \sim 4$; (d) $\varepsilon \sim 8$; and (e) $\varepsilon \sim 12$.

the second mechanism (Fig. 17b) in the early stages of processing that provides the higher rate of misorientation increment with strain (Fig. 16) and the final formation of more uniform recrystallized structure.

This is caused by the fact that the formation of subgrain structure through the first mechanism requires the long-range rearrangement of lattice dislocations, while the second process requires short-range rearrangement of lattice dislocations. Therefore, the first mechanism is observed at high temperatures in dilute alloys containing no pinning agents [28], and the second mechanism plays a vital role in CDRX initiation at intermediate temperature in aluminum alloys containing a dispersion of nanoscale particles. The 5024 alloys contain coherent $Al_3(Sc,Zr)$ dispersoids, which are highly effective in pinning lattice dislocations [20,32,33]. In addition, the rearrangement of lattice dislocation in Al–Mg alloys at 300 °C can occur through slow low-temperature climb [34]. This is why, the increase in the misorientation of LABs, which delimit equiaxed subgrains (Fig. 17a), occurs at a very low rate and the misorientation attains an apparent plateau, which can be obtained by extrapolation at $\varepsilon \geq 2$ [22] (Fig. 16).

Therefore, in the AA5024 alloy at the intermediate temperature, the rearrangement of lattice dislocations over large distances is restricted, and the formation of 3D arrays of LABs can occur through the initial formation of deformation bands, mainly [8,19,22–24,35,36]. The second mechanism contributes significantly to the evolution of 3D arrays of deformation LABs [19] if single slip is dominant [28]. Simple shear is favorable for single slip operation. Therefore, BP provides uniformity of simple shear in such strain hardening material [10,17] as the AA5024 alloy [5] that strongly facilitates the formation of deformation bands during first and second pressings. Significant broadening of the shear zone and an increasing contribution of simple shear to the overall strain due to BP [1,15,37] provides the uniform formation of numerous planar GNBs. Upon further strain the lattice dislocations rearrange quickly over short-range distances within and the planar LABs [31]. As a result, a lamellar structure substitutes the banded structure. This process provides the high rate of CDRX in Stage II (Fig. 16). Finally, chains of recrystallized grains evolve (Fig. 17c).

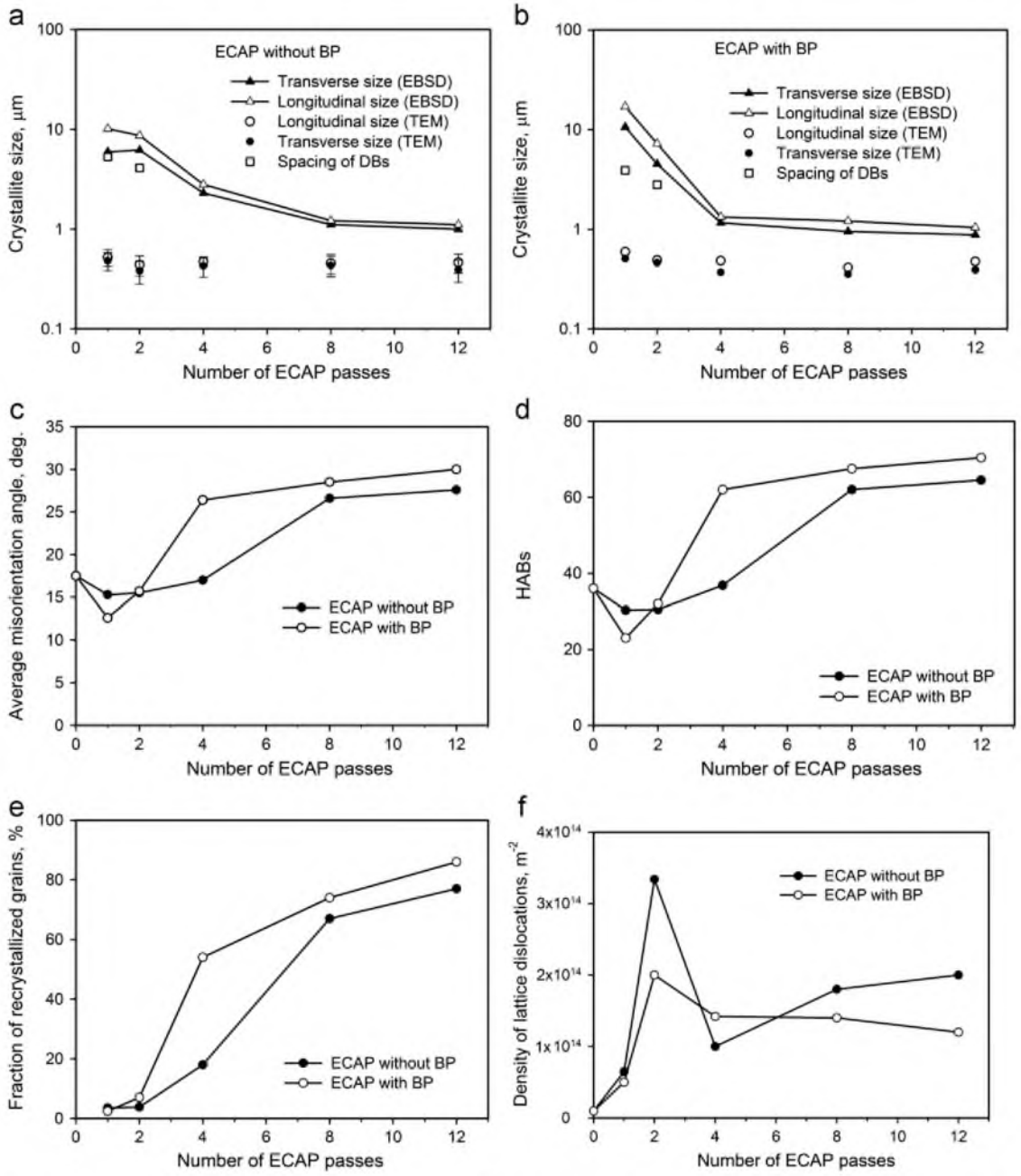

Fig. 15. Effect of strain on crystallite size (a and b), average misorientation angle (c), population of HABs (d), fraction of recrystallized grains (e), and density of lattice dislocations (f).

At $\varepsilon \leq 2$ in Stage I (Fig. 16), most lattice dislocations are consumed for the formation of GNBs. However, the rate of this process is not sufficient to consume all lattice dislocations for the formation of deformation bands; the extensive accumulation of lattice dislocations takes place within the interiors of original grains (Fig. 15f). The formation of GNBs is highly accelerated due to the application of BP. As a result, CDRX occurs at a high rate (Figs. 15c–e and 16) and a lower density of individual dislocations is accumulated (Fig. 15f). Thus, incorporating BP increases the fraction of lattice dislocations emitted by sources, which are consumed for the formation of HABs due to two factors. First, the spacing of GNBs strongly decreases due to the incorporation of BP, and the lattice dislocations acquire the ability rearrange by climb to form short transverse LABs (Fig. 17b). Second, the planar deformation of moderate-to-high boundaries, which originated from GNBs, are able to trap almost all lattice dislocations crossing the interiors of deformation bands (Fig. 17c), yielding a high rate of their transformation into HABs upon further strain. As a result, a significant acceleration of the CDRX process takes place in Stage II (Fig. 16) with increasing strain from ~2 to ~4 due to incorporation of BP, and a drop in dislocation density is observed (Fig. 15f). The number of lattice dislocations emitted by sources becomes less than the number of dislocations trapped by deformation boundaries, which increases their misorientation at a high rate. In contrast, the deviation from simple shear hinders CDRX under ECAP without BP; numerous lattice dislocation emitted by sources are not consumed by deformation boundaries to increasing their misorientations, and a slow growth in lattice dislocation density is observed in Stage II under ECAP without BP.

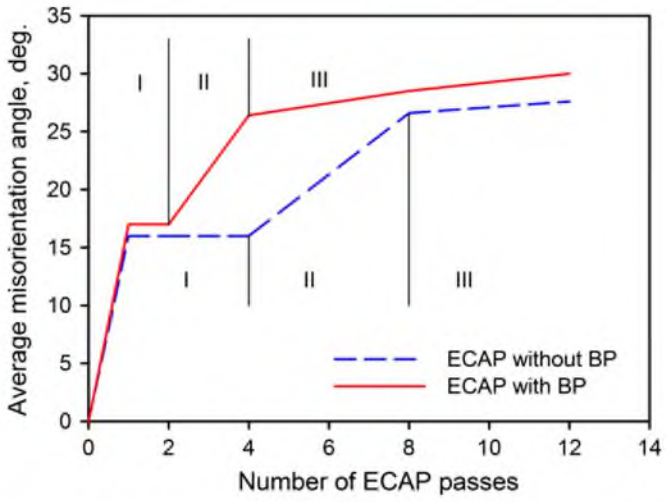

Fig. 16. Schematic drawing of the relationship between the average misorientation angle and number of ECAP passes.

The facilitation of deformation banding by incorporating BP plays a key role in attaining a fully recrystallized structure. Under ECAP without BP, the numerous initial grains, which are not favorably oriented for the formation of the deformation bands, remain unrecrystallized because deformation banding is hindered within them. The application of BP allows for deformation banding within the unrecrystallized grains, further triggering conversion into true submicron-scale grains. As a result, a fully recrystallized structure evolves under ECAP with BP and only a partially recrystallized structure evolves under ECAP without BP. BP induces the difference between the average misorientation and recrystallized fraction in Stage because some unrecrystallized remains of the initial grains are highly resistant to their subdivision by GNBs under ECAP without BP up to high strains. It is apparent that the formation of more uniform UFG structure due to BP provides both uniformity of microhardness distribution through the cross-sectional planes of the billet and a small increment in hardness as well.

Thus, there exist three clear advantages in imposing a BP. First, BP greatly promotes grain refinement under ECAP in Sc-containing Al–Mg alloys at intermediate temperature, accelerating the formation of deformations bands. Second, simple shear improves homogeneity in the formation of deformation bands throughout the entire bodies of workpieces. As a result, billets processed by ECAP with BP exhibit excellent homogeneity in deformation structure and microhardness. Third, the application of BP eliminates pressing defects. Therefore, ECAP with BP is highly attractive for commercial implementation.

5. Conclusion

1. Samples of a 5024 alloy were processed by equal channel angular pressing with and without back pressure for up to twelve passes at $T=300\ ^{\circ}C$. Incorporating back pressure allows for the fabrication of defect-less workpieces with a high level of homogeneity.
2. The equal channel angular pressing of AA5024 with and without back pressure at 300 °C to a total strain of 12 allows for the formation of fully and partially recrystallized structures, respectively, with an average grain size of $\sim 0.9\ \mu m$. Recrystallized grains contain a relatively high density of lattice dislocations ($\rho \sim 2 \times 10^{14}\ m^{-2}$). The boundaries of recrystallized grains are almost free of grain boundary dislocations.

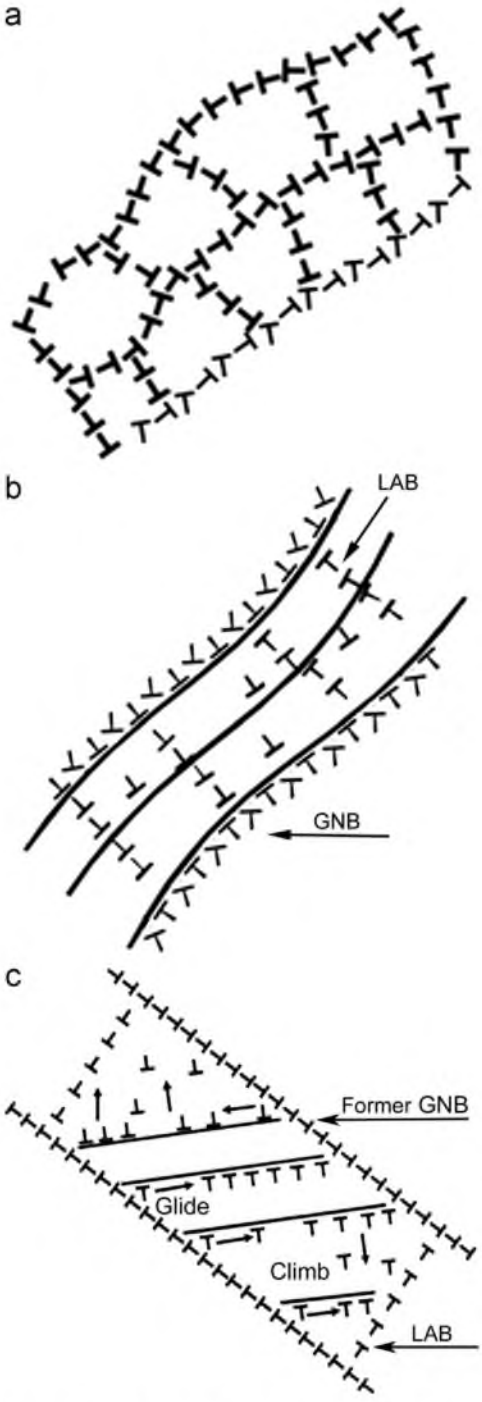

Fig. 17. Schematic representation of CDRX mechanism: (a) the formation of arrays of aquiaxed subgrains; (b) the formation of lamellar arrays of subgrains; and (c) interaction of low-angle boundaries with lattice dislocations resulting in a progressive increase in their misorientation.

3. Microstructural evolution during equal channel angular pressing occurs through continuous dynamic recrystallization. The application of a back pressure highly facilitates the formation of deformation bands delimited by low-angle boundaries along the shear direction during the first 2 passes through the die. Further deformation leads to the transformation of these boundaries into high-angle boundaries at a high rate allowing for the formation of a fully recrystallized structure at $\varepsilon \sim 12$.

Acknowledgments

This study was supported by the Federal Agency for Science and Innovations, Russia, under Grant No. 02.740.11.0510. The main results were obtained by using equipment at the Joint Research Center, Belgorod State University.

References

[1] R.Z. Valiev, T.G. Langdon, Prog. Mater. Sci. 51 (2006) 881–981.
[2] O. Sitdikov, T. Sakai, E. Avtokratova, R. Kaibyshev, Y. Kimura, K. Tsuzaki, Mater. Sci. Eng. 444 (2007) 18.
[3] O. Sitdikov, T. Sakai, E. Avtokratova, R. Kaibyshev, K. Tsuzaki, Y. Watanabe, Acta Mater. 56 (2008) 821–834.
[4] M. Furukawa, A. Utsunomia, K. Matsubara, Z. Horita, T.G. Langdon, Acta Mater. 49 (2001) 3829–3838.
[5] R. Kaibyshev, A. Mogucheva, A. Dubyna, Mater. Sci. Forum 706-709 (2012) 55–60.
[6] A. Vinogradov, A. Washikita, K. Kitagawa, V.I. Kopylov, Mater. Sci. Eng. A349 (2003) 318–326.
[7] F. Musin, R. Kaibyshev, Y. Motohashi, G. Itoh, Metall. Mater. Trans. 35A (2004) 2383–2392.
[8] P.J. Apps, J.R. Bowen, P.B. Prangnell, Acta Mater. 51 (2003) 2811–2822.
[9] R.Ye. Lapovok, J. Mater. Sci. 40 (2005) 341–346.
[10] R.K. Oruganti, P.R. Subramanian, J.S. Marte, M.F. Gigliotti, S. Amancherla, Mater. Sci. Eng. A 406 (2005) 102–109.
[11] Ch. Xu, M. Furukawa, Z. Horita, T.G. Langdon, Mater. Sci. Eng. A 398 (2005) 66–76.
[12] S. Ferrasse, V.M. Segal, F. Alford, J. Kardokus, S. Strothers, Mater. Sci. Eng. A 493 (2008) 130–140.
[13] P.W.J. Mckenzie, R. Lapovok, Y. Estrin, Acta Mater. 55 (2007) 2985–2993.
[14] P.W.J. Mckenzie, R. Lapovok, Acta Mater. 58 (2010) 3212–3222.
[15] A. Hasani, R. Lapovok, L.S. Toth, A. Molinari, Scr. Mater. 58 (2008) 771–774.
[16] R. Kaibyshev, D. Tagirov, A. Mogucheva, Adv. Eng. Mater. 12 (2010) 735–739.
[17] Ch. Xu, K. Xia, T.G. Langdon, Acta Mater. 55 (2007) 2351–2360.
[18] F. Kang, J.T. Wang, Y.L. Su, K.N. Xia, J. Mater. Sci. 42 (2007) 1491–1500.
[19] R. Kaibyshev, K. Shipilova, F. Musin, Y. Motohashi, Mater. Sci. Eng. A 396 (2005) 341–351.
[20] G. Tomas, M.J. Goringe, Transmission Electron Microscopy of Metals, Wiley, New York, 1979.
[21] M. Mabuchi, K. Ameyama, H. Iwasaki, K. Higashi, Acta Mater. 47 (1999) 2047–2057.
[22] I. Mazurina, T. Sakai, H. Miura, O. Sitdikov, R. Kaibyshev, Mater. Sci. Eng. A 473 (2008) 297–305.
[23] I. Mazurina, T. Sakai, H. Miura, O. Sitdikov, R. Kaibyshev, Mater. Sci. Eng. A 486 (2008) 662–671.
[24] I. Mazurina, T. Sakai, H. Miura, O. Sitdikov, R. Kaibyshev, Mater. Trans. 50 (2009) 101–110.
[25] F.J. Humphreys, M. Hatherly, Recrystallization and Related Annealing Phenomena, Elsevier, Oxford, 2004.
[26] H. Jazaeri, F.J. Humphreys, Acta Mater. 52 (2004) 3239–3250.
[27] H.W. Zhang, X. Huang, R. Pippan, N. Hansen, Acta Mater. 58 (2010) 1698–1707.
[28] R. Kaibyshev, in: C. Bettles, M. Barnett (Eds.), Advances in Wrought Magnesium Alloys: Properties, Processing and Applications, Woodhead Publishing Limited, Cambridge, 2012, pp. 186–226.
[29] E. Martin, J.J. Jonas, Acta Mater. 58 (2010) 4253–4266.
[30] D.A. Hughes, N. Hansen, D.J. Bammann, Scr. Mater. 48 (2003) 147–153.
[31] A. Belyakov, T. Sakai, R. Kaibyshev, Metall. Mater. Trans. 29 (1998) 161–167.
[32] J. Røyset, N. Ryum, Int. Mater. Rev. 50 (2005) 19–44.
[33] T.G. Nieh, L.M. Hsiung, J. Wadsworth, R. Kaibyshev, Acta Mater. 46 (1998) 2789–2800.
[34] R. Kaibyshev, F. Musin, E. Avtokratova, Y. Motohashi, Mater. Sci. Eng. A 392 (2005) 373–379.
[35] P.J. Apps, M. Berta, P.B. Prangnell, Acta Mater. 53 (2005) 499–511.
[36] Y. Huang, J.D. Robson, P.B. Prangnell, Acta Mater. 58 (2010) 1643–1657.
[37] R. Lapovok, L.S. Toth, A. Molinari, Y. Estrin, J. Mech. Phys. Solids 57 (2009) 122–136.